Thesis for the degree of Master of Science

Effects of Optical Filtering on Signal Characterization in Coherent Systems

Henrik Eliasson

CHALMERS

EXFO Sweden AB
Arvid Hedvalls Backe 4

Photonics Laboratory
Department of Microtechnology and Nanoscience
Chalmers University of Technology

SE-41296 Göteborg, Sweden, 2012

Effects of optical filtering on signal characterization in coherent systems

Henrik Eliasson

Photonics Laboratory
Department of Microtechnology and Nanoscience
Chalmers University of Technology
SE–412 96 Göteborg
Sweden
Telephone: +46–(0)31–772 10 00

Printed in Sweden by
Reproservice
Chalmers Tekniska Högskola
Göteborg, Sweden, 2012

Cover caption: TR-EVM plots of QPSK signals at 28 GBaud with increasingly narrow optical filtering applied. The first image shows the unfiltered signal, the second and third image shows the signal filtered with a 42 and 18 GHz FWHM Gaussian optical filter. The concept of TR-EVM is explained in sections 2.5.1 and 2.5.2.

Abstract

There is a big need for standardizing signal quality tests of transmitters for 100 Gb/s PM-QPSK fiber optic communication systems. Such systems are currently being deployed and still, there is no standard for transmitter testing. Several approaches for doing this in an efficient manner have been proposed. These include different methods of detecting the signal and different approaches for filtering the signal. The signal can be sampled electrically or optically, both over- and undersampled. The choices of filtering range from optical and electrical hardware filters to filtering in digital signal processing. All filtering and sampling techniques are not compatible.

The focus in this project will be on optical filtering that can be used together with optical sampling. The reason for using optical sampling is to achieve high measurement bandwidth. The only filtering technique which is easily applicable when sampling optically is optical filtering. This is because the signal is undersampled. The project is an exploratory study to investigate if optical sampling together with optical filtering is a good approach for signal quality testing. Experiments were made to assess the accuracy of optical filtering by measuring on QPSK signals and comparing to DSP filtered measurements. Impulse response measurements were also made to compare the impulse responses of an optically and DSP filtered system. Also, theoretical work has been done to determine the equivalence to optical filtering in the DSP domain. The accuracy of the optical filtering is found to be sufficient under certain conditions on the filter characteristics. It is found that optical filtering together with optical sampling is a viable method for fast and efficient transmitter testing. The optical filtering method should be included in future standardization studies as an alternative to DSP filtering used in real-time sampling approaches.

Acknowledgement

I am very fortunate to have been supervised and helped in this project by such competent people. All of you have both inspired and learned me so much. I want to thank the crew at EXFO Sweden, Mathias Westlund, Henrik Sunnerud and Mats Sköld. I also want to thank Pontus Johannisson who have been my examiner at the Photonics Laboratory. Pontus has helped me very much in understanding the finer mathematical details of signals and how they can be described and manipulated. Also he has provided invaluable support in writing the report. Mats Sköld learned me a lot about digital signal processing algorithms and gave many good advice on how to write the programs that were used in the experiments. I worked a lot in the lab together with Henrik Sunnerud, an incredibly educative experience. Mathias Westlund has been my main supervisor, it has always been possible to ask questions and get good answers, be it discussions on career possibilities or fiber optics. All have been generous with their time and always helped out.

I chose to do my thesis project at EXFO Sweden beacuse I wanted to get a picture of how it is to work with research and development at a high-tech company. I feel like this was fulfilled. It has been ever so fun to listen to meetings with brainstorming for new products or solutions. The most fun however must have been to hear of the different strategies for haggling to get down the price of the latest ADC circuit by playing the different providers against each other.

Finally I would like to aim some warm feelings towards my girlfriend Sofie. You always help me get my confidence back when things are difficult.

Henrik Eliasson

Abbreviations used in the text

ADC	Analog-to-digital converter
ASE	Amplified stimulated emission
AWG	Arrayed waveguide grating
BER	Bit error rate
CW	Continuous wave
DSP	Digital signal processing
EDFA	Erbium-doped fiber amplifier
EVM	Error vector magnitude
GSOP	Gram-Schmidt orthogonalization procedure
HW	Hardware
I	In-phase
IF	Intermediate frequency
ISI	Inter-symbol interference
LCoS	Liquid crystal on silicon
LO	Local oscillator
OMA	Optical modulation analyzer
OSA	Optical spectrum analyzer
PM	Polarization multiplexing
PRBS	Pseudo random binary sequence
Q	Quadrature
QAM	Quadrature amplitude modulation
QPSK	Quadrature phase-shift keying
RMS	Root mean square
SP	Single polarization
TR-EVM	Time-resolved error vector magnitude
WDM	Wavelength division multiplexing

Contents

Chapter 1

Introduction

In the 1960s, Charles K. Kao and his co-workers did the groundbreaking work of transmitting light in optical fibers with low loss of optical power. They were the first to realize that the previously achieved high losses arose from impurities in the fiber. In 1965 they concluded that the fundamental limit for optical fiber loss was below 20 dB/km [1]. Today, optical fibers with loss below 0.17 dB/km are commercially available [2]. This discovery together with the development of other key technologies such as semiconductor lasers and the Erbium-doped fiber amplifier (EDFA) makes it possible to transmit digital data at high data rates over long distances using optical fibers [3], [4].

The first fiber optic communication systems transmitted data using on-off keying, i.e. letting presence of light represent a binary 1 and absence of light represent a binary 0. This kind of primitive modulation was used for a very long time due to its excellent noise tolerance and low transmitter/receiver complexity. It is first in recent years that more advanced modulation formats have been employed in order to achieve higher bit rates and improved spectral efficiency. The most recent advances in fiber optic communications being the use of coherent receivers and advanced modulation formats like M-ary phase-shift keying, M-PSK, and quadrature amplitude modulation, M-QAM. Further improvements can be achieved by utilizing both polarizations through the use of polarization multiplexing, PM, or polarization shifting, PS [5]. For systems which require higher data rates, many optical carriers at different wavelengths are transmitted in the same fiber, this is called wavelength division multiplexing, WDM. The use of a coherent receiver which can detect both phase and amplitude of the optical signal also opens up to the use of digital signal processing, DSP, to correct for non-idealities in the receiver and transmission impairments like fiber dispersion and laser phase noise [6].

At the moment, a new generation of fiber optic networks is being deployed. This new generation utilizes advanced modulation formats like PM-QPSK and coherent receivers with DSP to achieve data rates of 100 Gb/s on each optical carrier. Still there are no standards on how to characterize the signal quality in these systems. This thesis will focus on the filtering of the signal that is done when characterizing the signal and the different filter implementations that are possible, both optical and electrical. There are many ways of filtering the signal, it can be done in the optical domain to remove amplified spontaneous emission (ASE), noise coming from the EDFA or in digital signal processing (DSP) to improve sensitivity by removing noise.

1.1 Motivation for this project

Using optical filters becomes the only alternative when the signal is detected using optical sampling. Because of the undersampling typically involved in optical sampling it is not straight forward to filter the signal in DSP. DSP filtering of undersampled data requires pattern data and using measurements from consecutive patterns to rebuild the waveform. The aim of this master thesis project is to work towards developing an approach to characterize the signal quality with signal filtering done in the optical domain. The first step is to determine if there are suitable optical filters with regard to tunability, bandwidth, and frequency response to name a few relevant properties. Then it has to be established theoretically and proved experimentally what the equivalence to optical filtering is in terms of electrical filtering. It also has to be proven experimentally that the optical filters fulfill the criteria put on them. The final step is then to suggest how a signal quality characterization standard utilizing optical filtering could look. The project will build on earlier work by EXFO Sweden AB and use concepts which are implemented in their optical modulation analyzers (OMA). The project will contain theoretical, experimental, and numerical work.

The international standardizing organizations are looking at defining a standard for pass/fail testing transmitters for next generation 100 Gb/s networks. There are several approaches to testing transmitters, using optical sampling with optical filtering being one of them, however studies has not been done which look at the combination of optical filtering and optical sampling for this purpose. It is therefore important to establish if this is a possible route towards a new standard. For previous generations of fiber optic communications systems, the standards for transmitter testing have specified filtering in the electrical domain. Typically a fourth order Bessel filter with a 3-dB electrical bandwidth of 0.75×symbol rate has been used [7].

The project is done at EXFO Sweden AB and the Photonics Laboratory, Department of Microtechnology and Nanoscience, Chalmers University of Technology. EXFO is an industry leader in measurement equipment for fiber optic communication networks and a manufacturer of equipment for transmitter/signal testing utilizing optical sampling technology.

1.2 Organization of the report

Chapter 2 contains an overview of coherent detection, optical sampling, and how these technologies could be used to measure signal quality. In chapter 3, the digital signal processing which is involved with coherent detection is discussed. A short summary of possible optical filtering technologies and the theoretical description of filters follows in chapter 4. How the experiments were performed and descriptions of the numerical simulations are discussed in chapter 5. Finally the results of the experiments and conclusions which can be drawn are in chapters 6 and 7.

Chapter 2

Coherent detection

The word coherent is used in this context to describe a receiver that can detect both the amplitude and phase of the received light electric field. Since a photo detector is sensitive only to the intensity of the incoming light, the signal is mixed with a local oscillator in order to retrieve phase information. Exactly how this is done is described in further detail in section 2.1.

Optical sampling is a technique which can be used together with coherent detection to achieve very high bandwidth by utilizing a pulsed local oscillator. The bandwidth is then determined by the length of the optical pulses. When using optical sampling it is often advantageous to filter the signal optically, an explanation of this and a brief description of the technique follows in section 2.3.

2.1 The 90° hybrid receiver

A complete mapping of the optical fields amplitude and phase to the electrical domain is very appealing since it opens up to using advanced modulation formats and DSP to correct for signal impairments. This is achieved by mixing a local oscillator (LO) laser with the signal in a 90° hybrid. The 90° hybrid is built up by four 3-dB couplers with a 90° phase delay on one of the intermediate arms. The hybrid is followed by balanced detectors to separate the in-phase, I, and quadrature, Q, components. The I and Q components are the real and imaginary part of the field in phasor notation [8]. Fig. 2.1(a) shows the components together with the input and output signals.

The expressions for the input fields are

$$E_s(t) = u(t)e^{i(\omega_s t+\phi_s(t))} \tag{2.1}$$

and

$$E_{LO}(t) = v(t)e^{i(\omega_{LO} t+\phi_{LO}(t))}, \tag{2.2}$$

where $u(t)$ is the baseband signal representing the complex valued data symbols and $v(t)$ is the real valued amplitude of the LO. The frequencies ω_s and ω_{LO} are the optical frequencies of the transmitter laser and the local oscillator laser. The phase noise is represented by the functions $\phi_s(t)$ and $\phi_{LO}(t)$ due to the finite linewidth of the transmitter and LO lasers.

The fields at the outputs of the hybrid are found by superposing the contributions from the input fields E_S and E_{LO}. The contribution from each input field is found by repeated application of Fig. 2.1(b). The output fields are given by

$$E_1 = \frac{1}{2}\left(E_s + jE_{LO}\right), \qquad E_2 = \frac{1}{2}\left(jE_s + E_{LO}\right), \tag{2.3}$$

$$E_3 = \frac{j}{2}\left(E_s - E_{LO}\right), \qquad E_4 = \frac{-1}{2}\left(E_s + E_{LO}\right). \tag{2.4}$$

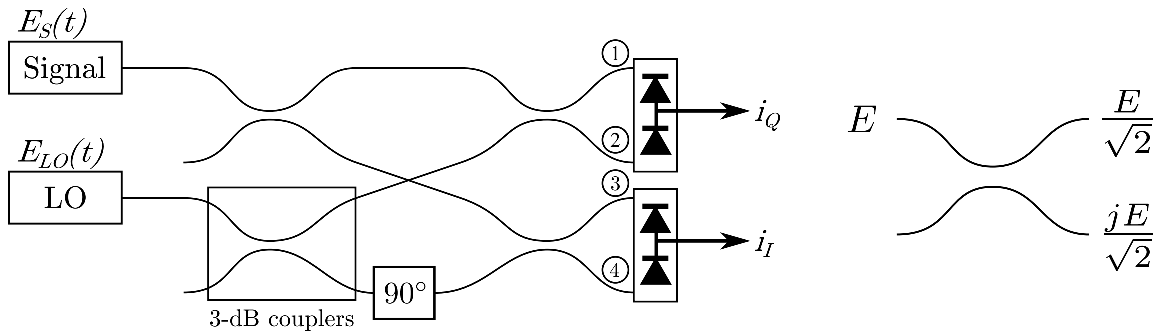

(a) (b)

Figure 2.1: Detailed figures of the 90° hybrid and the 3-dB coupler. (a) Schematic layout of the 90° hybrid with attached balanced detectors. (b) Output fields as functions of input field E in a 3-dB coupler.

The output photocurrent of a diode detector is given by $i_{out} = R|E_{in}|^2$ where R is the responsivity [A/W] of the diode detector. Calculating the output photocurrents from port 1 and 2 using $|z|^2 = zz^*$ and $\Im(z) = \frac{1}{2j}(z - z^*)$ we get

$$i_1 = R|E_1|^2 = \frac{R}{4}|E_s + jE_{LO}|^2 = \frac{R}{4}\left[|E_s|^2 + |E_{LO}|^2 + 2\Im\left(E_{LO}^* E_s\right)\right], \tag{2.5}$$

$$i_2 = R|E_2|^2 = \frac{R}{4}|jE_s + E_{LO}|^2 = \frac{R}{4}\left[|E_s|^2 + |E_{LO}|^2 - 2\Im\left(E_{LO}^* E_s\right)\right], \tag{2.6}$$

$$i_3 = R|E_3|^2 = \frac{R}{4}|jE_s - jE_{LO}|^2 = \frac{R}{4}\left[|E_s|^2 + |E_{LO}|^2 - 2\Re\left(E_{LO}^* E_s\right)\right], \tag{2.7}$$

$$i_4 = R|E_4|^2 = \frac{R}{4}| - E_s - E_{LO}|^2 = \frac{R}{4}\left[|E_s|^2 + |E_{LO}|^2 + 2\Re\left(E_{LO}^* E_s\right)\right]. \tag{2.8}$$

Subtracting i_2 from i_1 and i_3 from i_4 gives us outputs i_Q, i_I and the final output i as

$$i_Q = i_1 - i_2 = R\Im\left(E_{LO}^* E_s\right) = R|u(t)||v(t)|\sin\left[(\omega_{LO} - \omega_s)t + \phi_{LO}(t) - \phi_s(t) + \arg(u(t))\right], \tag{2.9}$$

$$i_I = i_4 - i_3 = R\Re\left(E_{LO}^* E_s\right) = R|u(t)||v(t)|\cos\left[(\omega_{LO} - \omega_s)t + \phi_{LO}(t) - \phi_s(t) + \arg(u(t))\right] \tag{2.10}$$

and

$$i = i_I + ji_Q = RE_{LO}^* E_s. \tag{2.11}$$

If we set $\omega_{IF} = \omega_{LO} - \omega_s = 0$ and $\phi(t) = \phi_{LO}(t) - \phi_s(t) = 0$ we see that i_Q and i_I are linear mappings of $|u(t)|\sin[\arg(u(t))] = \Im(u(t))$ and $|u(t)|\cos[\arg(u(t))] = \Re(u(t))$. Adding up the two outputs according to equation 2.11 we get a linear mapping of $u(t)$, assuming that $v(t)$ is a constant. Compensating for these variables being non-zero and varying over time is something which can be done in DSP so that we get the linear mapping sought after. Also note that this means that the hybrid receiver with DSP in the ideal case mixes down the signal so that the signal spectrum is zero centered.

2.2 The QPSK modulation format

In this report the focus will be on the quadrature phase shift keying (QPSK) modulation format. The reason for this being that it is the modulation format which will be used in the 100 Gb/s

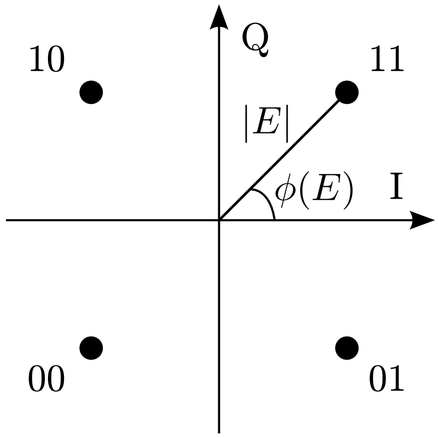

Figure 2.2: A QPSK constellation diagram. $|E|$ is the electric field amplitude and ϕ is the phase of the electric field.

networks which are beginning to be employed. QPSK-modulation means encoding the binary information on the phase of the light, with the signal having four different phase states. It is also possible to use higher order phase shift keying, like 8-PSK where the data is encoded on 8 different phase states. Usually QPSK is used together with polarization multiplexing, i.e. by transmitting independent QPSK-data in both polarizations. A modulation format is often visualized with a constellation diagram which is a 2-D plot where the symbols are represented in the complex plane with phase and amplitude. A constellation diagram for QPSK is shown in Fig. 2.2.

2.3 Optical sampling

Optical sampling is a method for increasing the measurement bandwidth by using an LO consisting of short light pulses. The price paid is often that the signal is undersampled, i.e. sampled at a rate lower than the Nyquist rate. However, this is not always the case and optical sampling at rates above the Nyquist rate has also been performed [9]. The main motivation behind this section is to make clear why optical filtering is the only practical alternative. Also the relation between sampling rate and bandwidth will be made clearer.

In the case of coherent detection with a 90° hybrid receiver, optical sampling can be done by utilizing a pulsed LO laser. For simplicity we assume that the pulses from the LO laser do not overlap. The LO field can be represented on the form

$$E_{LO}(t) = v(t)e^{i(\omega_{LO}t+\phi_{LO}(t))} \tag{2.12}$$

where $v(t)$ in this case represents a real valued pulse train. The pulse train can be described as

$$v(t) = \sum_{k=-\infty}^{\infty} f(t-t_k) \tag{2.13}$$

where $f(t)$ is an arbitrary narrow pulse and $t_k = k/f_{sampling}$. Between the pulses, where $E_{LO} \approx 0$, the output from the receiver will be zero as can be seen in Eqs. 2.9 and 2.10. Effectively this means that the field E_s will be sampled only during the very short pulse time which is equivalent to having a high bandwidth. The outputs i_I and i_Q are then sampled synchronously with the LO pulses. The technique is called optical sampling even though it involves both optical and electrical sampling.

If the sampling is done at a rate below the Nyquist rate there is no way to fully reconstruct the received signal field and spectrum, which is required to filter the signal in DSP. There are ways to get around this, by transmitting a fixed data pattern periodically, one can reconstruct the field of this pattern by using samples from consecutive data patterns. For unknown data or very long patterns this is not possible. For very long patterns, longer than approximately 2^{15}, it is impossible in practice because of the requirements on memory depth and computing power. This is the reason why optical filtering is preferred when the signal is optically sampled, it requires no such tricks and the filtering can be applied independently on the transmitted data.

2.4 Electrical sampling

The most common competing technique to optical sampling is to use a continuous wave (CW) LO and detect the signal from the balanced detectors using real-time electrical sampling. This puts very tough requirements on the ADC bandwidth and sampling rate. According to the Nyquist sampling theorem, the sampling rate has to be at least two times the single sideband bandwidth of the signal spectrum in order to retrieve the full signal waveform. The bandwidth has to be sufficiently wide so that the signal spectrum has fallen off significantly at the ADC bandwidth. The requirements on the ADC lead to this solution being difficult or impossible.

The advantage of this approach is that the optical field is sampled in real time. This gives us the possibility of doing more in DSP, including filtering of the signal. For a real-time electrically sampled system it is possible to filter the signal in the optical, electrical or DSP domain.

It is also possible to detect the signal with electrical undersampling, i.e. by having an ADC with high bandwidth but lower sampling rate. This is typically achieved by having a track-and-hold circuit before a low sampling rate ADC. A track-and-hold circuit tracks the signal and holds the output fixed at the sampled voltage between samples.

2.5 Signal quality characterization

Traditionally, the quality of signals in fiber optic communication systems have been characterized by eye diagrams, which is an excellent approach for on-off keyed signals. Looking at the opening of the eye diagram at the decision points gives a quick measure of the signal quality. For multi-level modulation formats it is not enough to have a single eye diagram but it is still possible to plot eye diagrams for the I and Q part of the signal separately. An alternative approach is to use the error vector magnitude (EVM), a measure that contains information about both I and Q deviations from the ideal. An extension of the EVM concept is time-resolved EVM (TR-EVM), which also gives information about the transitions between symbols. Using masks together with TR-EVM could prove to be a good way of pass/fail testing transmitters. These concepts will be explained in the following sections.

2.5.1 Error vector magnitude

The EVM concept is very closely related to signal to noise ratio (SNR) [10]. In some sense, both say something about the relation between noise and signal levels. It is a measure of the distance between an ideal reference symbol and the measured symbol in the I-Q plane. The first step is to define the error vector. An illustration of this is shown in Fig. 2.3. If the measured and correct symbols are given as complex numbers this can be expressed as

$$e = \hat{s} - s, \tag{2.14}$$

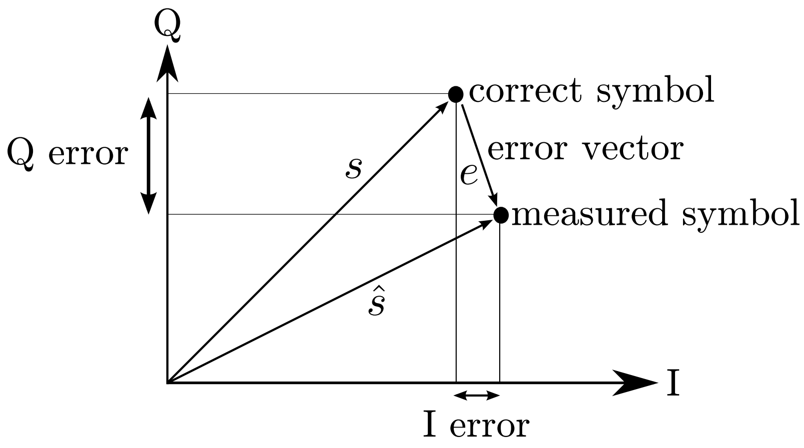

Figure 2.3: The concept of error vector.

where e is the error vector, $\hat{s}$ the measured symbol, and s the correct symbol. The error vector magnitude is then defined as

$$\text{EVM} = \frac{|e|}{|s_{max}|} = \frac{|\hat{s} - s|}{|s_{max}|} = \frac{\sqrt{(\text{I error})^2 + (\text{Q error})^2}}{|s_{max}|}, \tag{2.15}$$

where the EVM has been normalized with respect to $|s_{max}|$ which is the maximum amplitude of the correct symbols. When talking about EVM, it is understood that the measurements are done at the decision points, in the middle of the symbol slots. Commonly the RMS of many consecutive EVM measurements is calculated to give a single value characterizing the distribution of noise and signal impairments. Characterizing the signal by averaging the EVM at the decision points does not give any information on how the transitions between symbol slots look. In order to take this into account we introduce the concept of time-resolved EVM (TR-EVM)

2.5.2 Time-resolved error vector magnitude

Making a time-resolved EVM (TR-EVM) plot from a series of measured EVM values requires timestamping of each sample. The data is then plotted with the EVM on the y-axis and t modulo t_{symb} on the x-axis, where t_{symb} is the symbol slot time. In a TR-EVM plot it is also possible to see signal impairments in the transitions between symbols caused by the transmitter [11].

These impairments do not necessarily affect the bit error rate (BER) over a good data channel with high SNR and no nonlinearities. For more difficult channels like long haul optical fibers with low SNR and nonlinear signal distortion, the impairments could make a difference. A typical TR-EVM plot is presented in Fig. 2.4. All samples are plotted with their position in the symbol slot on the x-axis and the sample EVM on the y-axis. There are two different traces in the transitions reaching a maximum of 1 or $1/\sqrt{2}$. This is because the EVM in the transitions is different depending on if the transition passes through zero or not. Compare the transition from 11 to 00 and the transition from 11 to 01 in Fig. 2.2.

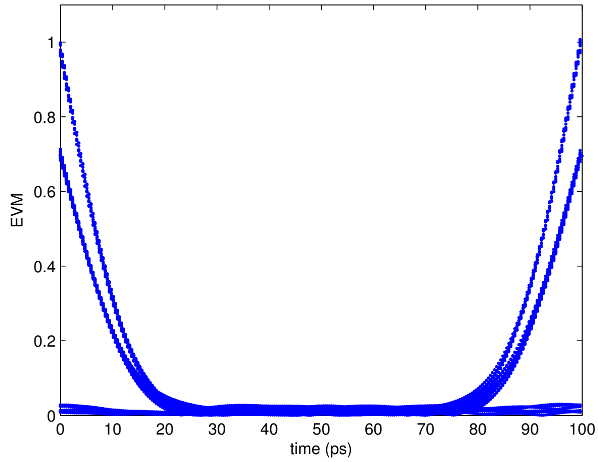

Figure 2.4: Computer simulated TR-EVM plot. The signal is modulated with QPSK at 10 GBaud with an OSNR of 30 dB. Filtering is done with a gaussian filter with 20 GHz FWHM bandwidth.

2.5.3 TR-EVM compared to a reference waveform

Another way of characterizing signal quality is to calculate the TR-EVM relative to a reference signal. If $E_{ref}(t)$ is the reference waveform and $E_{meas}(t)$ is the measured waveform, the TR-EVM compared to a reference is calculated as

$$\text{TR-EVM}_{ref}(t) = \frac{|E_{meas}(t) - E_{ref}(t)|}{|S|}, \tag{2.16}$$

where $|S|$ is the amplitude of the QPSK symbols. This approach can also be used to quantify the similarity between two signals by using one of the signals as $E_{ref}(t)$ and the other as $E_{meas}(t)$. The resulting TR-EVM$_{ref}$ is illustrated in the same way as TR-EVM by timestamping each sample over the symbol slot. The TR-EVM$_{ref}$ of a signal, which is perfectly identical to the reference, would be constant zero.

2.5.4 Mask testing

One reason for using the TR-EVM concept is to find masks which correlate well to bit error rate (BER) for pass/fail testing of transmitters. The mask is a geometric shape in the TR-EVM plot. The quality of the signal is then characterized by counting the number of samples which are inside the mask in the TR-EVM plot, these samples are called mask hits. A good signal will not have any samples inside the mask and a bad signal will have many mask hits. By choosing an appropriate mask together with appropriate filtering, this could allow for very quick testing of signal quality. The advantage of using masks and TR-EVM for signal characterization is that it in one step can take all signal impairments like skew, quadrature error and IQ-imbalance into account. An example of a mask in a TR-EVM plot is shown in Fig. 2.5. The samples are plotted in the same way as was described in section 2.5.2. The mask is chosen to somewhat resemble the shape of the TR-EVM plot so that an increase in EVM in the center region of the symbol slot would cause a mask hit.

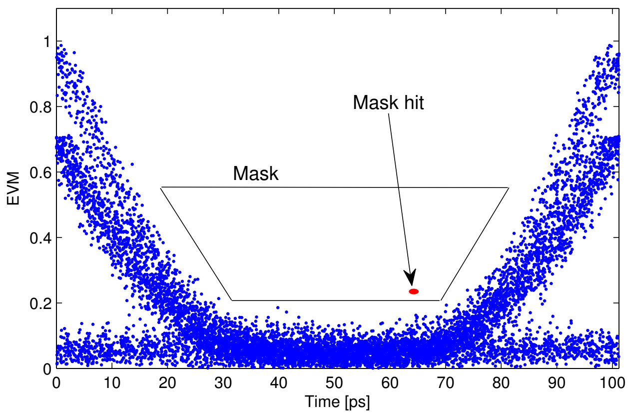

Figure 2.5: Measured TR-EVM plot with applied mask. One mask hit, which is marked.

Chapter 3

Digital signal processing

When looking at the measured $i = i_I + ji_Q$ plotted in the complex plane a few things are immediately clear. First of all, the constellation diagram is spinning due to ω_{IF}, ϕ_S and ϕ_{LO}. Second, the data points which should be on a circle are rather positioned on an ellipse which is somewhat slanted. This is an effect of the phase shift in the hybrid not being exactly 90°. Third, and not as easy to see, is that the transitions which should pass through zero might be a bit off, something that can be explained by a small timing mismatch between the I and Q channels. All of these effects can be corrected for in DSP to retrieve the baseband signal. Constellation diagrams of the detected signal before and after DSP is shown in Fig. 3.1(a). It should also be mentioned that all DSP algorithms which are described in this chapter are designed for real-time sampled systems.

Digital signal processing of the received signal is a big topic. Only the processing that was needed in the receiver software used in the experiments will be covered in this text. As an example, one of the parts of the DSP implementation that was omitted is compensation for chromatic dispersion. This was not required since all experiments were performed back-to-back. A block diagram of the different parts of the DSP is shown in Fig. 3.2. In all following sections except 3.7 it is assumed that the signal is modulated with QPSK.

3.1 I-Q channel timing correction

The digital sampling of the signal results in discrete measurements separated by a sampling interval time T_s. In general, the timing mismatch between the I and Q channel is not equal to an integer number of sampling intervals. This means one has to interpolate and resample the signal delayed by μT_s, where in general $\mu \in \mathbb{R}$. Usually μ is on the order of 1 or less but can in theory be any number. The situation is very different depending on where the timing mismatch comes from. If the I and Q channels of the transmitter are mismatched, the IF will cause the timing error to alternate between the received I and Q channels, making it very difficult to compensate for in DSP. On the other hand, if the timing error comes from, say, a longer electric cable on one of the receiver channels, the timing error will be constant on one of the channels and thus can be corrected for by delaying one channel. There are many ways of doing this and in the experiments it was done by interpolation with sinc functions. This is a conventional method for interpolation and gives a full reconstruction of the signal within the receiver bandwith. In this manner it is possible to correct for timing mismatches in offline processing. In the experiments, the delay was constant for all measurements. The delay was estimated manually and the same time delay was used to correct all measurements.

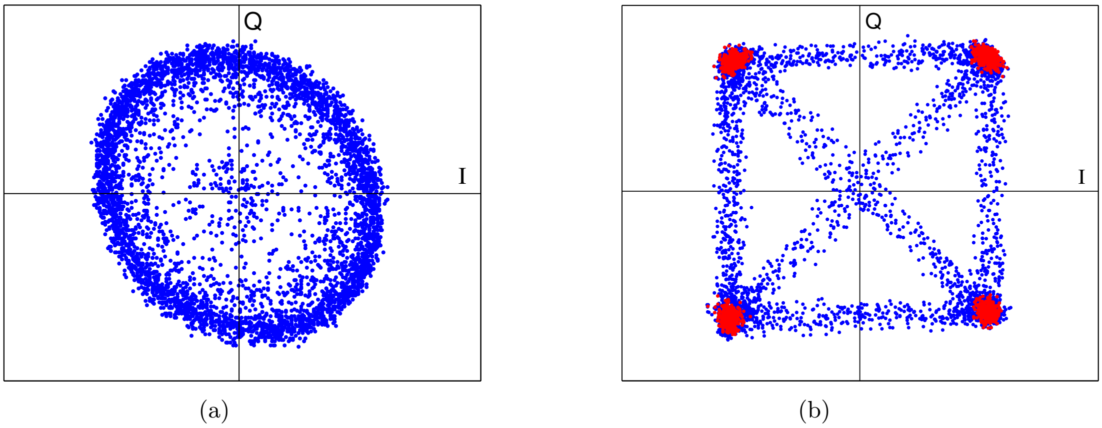

Figure 3.1: (a) The received signal before DSP. (b) The output after DSP, red marked samples are decision point samples.

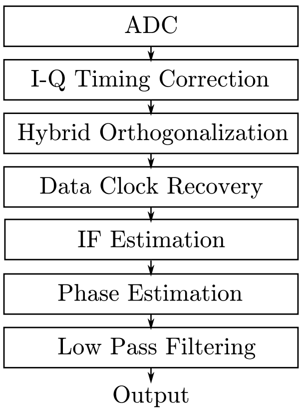

Figure 3.2: Block diagram of the constituents of the DSP system which were implemented in the receiver.

3.2 Hybrid orthogonalization

Correction of I-Q imbalance is the next step in the DSP. There are a few different algorithms to choose from, the simplest and most straightforward method is the Gram-Schmidt orthogonalization procedure (GSOP) [12]. While more advanced methods exist, which distribute the errors due to quantization noise more equally across I and Q channels, it will not be necessary in this case because of the small implications of quantization noise.

The orthogonalization is performed as follows. Start by calculating the correlation coefficient $\rho = \langle i_I(t) i_Q(t) \rangle$. Calculate the corrected I and Q values as

$$I(t) = \frac{i_I(t)}{\sqrt{P_I}} \tag{3.1}$$

and

$$Q(t) = \frac{1}{\sqrt{P_Q}} \left(i_Q(t) - \frac{\rho i_I(t)}{P_I} \right) \tag{3.2}$$

where

$$P_I = \left\langle i_I^2 \right\rangle, \tag{3.3}$$

$$P_Q = \left\langle \left(i_Q(t) - \frac{\rho i_I(t)}{P_I} \right)^2 \right\rangle \tag{3.4}$$

and $\langle\rangle$ denotes the mean value. The corrected signal $I(t) + jQ(t)$ will then form a circular shape in the complex plane. Again it should be noted that this algorithm is developed for QPSK and might have to be modified depending on the modulation format of the signal.

3.3 Clock recovery

The algorithms for removing the IF and phase noise require samples at the decision points, i.e. the center of the symbol slot. The first step in finding the field at the decision points is to find the symbol clock in the power spectrum of the received signal $\mathcal{F}\left(|i_I + ji_Q|^2\right)$. There will be a clearly visible spike in the power spectrum. The phase and frequency of that point in the spectrum will give the decision points. Finding the field at those points involve the same interpolation with sinc functions that was described in section 3.1.

It should be noted that this method is not adaptive and will not handle jitter very well. In the experiments performed for this thesis it was not a problem however since the transmitter was very stable and practically jitter free. Adaptive symbol clock recovery can be done by filtering out the clock spike in the power spectrum and finding the decision points based on the filtered signal.

3.4 Intermediate frequency estimation

This step is done to correct for $\omega_{IF} \neq 0$. The consequence of this is that $i = i_I + ji_Q$ will have a time dependent rotation in the complex plane. The direction of the rotation is determined by the sign of ω_{IF}. The purpose is to find a numeric estimation of ω_{IF} and use this value to correct for the rotation.

The estimation exploits the fact that all QPSK symbols in the complex constellation diagram will be transformed to the same point when taken to the power of four, this is shown in Fig. 3.3. The formula for estimating the intermediate frequency is [6]

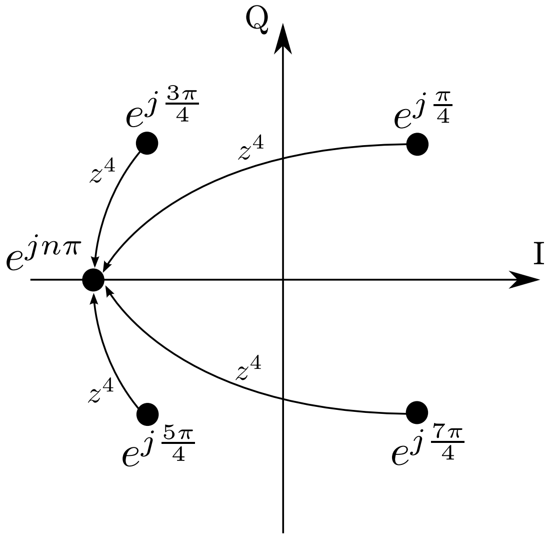

Figure 3.3: The power of four transformation of the QPSK symbols, n = 1,3,5,7.

$$\omega_{IF} = \frac{1}{4T_{sym}} \arg \left[\sum_{k=1}^{N} (S(k)S^*(k-1))^4 \right]. \tag{3.5}$$

Here $S(k)$ is the sequence of interpolated symbols, T_{sym} is the symbol slot time and N is the number of symbols. After finding ω_{IF}, the correction is done by multiplying $i(t)$ by $e^{-j\omega_{IF}t}$.

3.5 Phase estimation

After the intermediate frequency has been corrected for, there will still be residual phase noise left. The residual phase results from $\phi(t) = \phi_{LO}(t) - \phi_S(t)$ in equations 2.9 and 2.10. The residual phase at the decision points is calculated as [6]

$$\phi(k) = \frac{1}{4} \arg \left[\sum_{d=-D}^{D} S^4(k+d) \right]. \tag{3.6}$$

The number of samples taken into account for estimating the phase is $2D+1$, where D is the estimator depth. D decides how quick the response to phase changes will be. Choosing D is a trade-off between SNR tolerance and linewidth tolerance. With a low D, the estimator will respond quickly to rapid phase changes but will be sensitive to noise. A high D means resilience to noise but slow response to phase changes. If the phase noise goes outside the range $[-\pi, \pi]$, the resulting $\phi(k)$ will have to be unwrapped to get consistent data [13]. The whole procedure is referred to as the Viterbi-Viterbi algorithm [14].

3.6 Low-pass filtering

The low pass filtering in DSP was performed after IF and phase tracking. The reason for this was that the signal frequency spectrum before the tracking is not centered around zero. If the signal spectrum is not symmetric around zero when the filtering is applied there would be unwanted effects such as double transition rails in the constellation diagram. An illustration of double

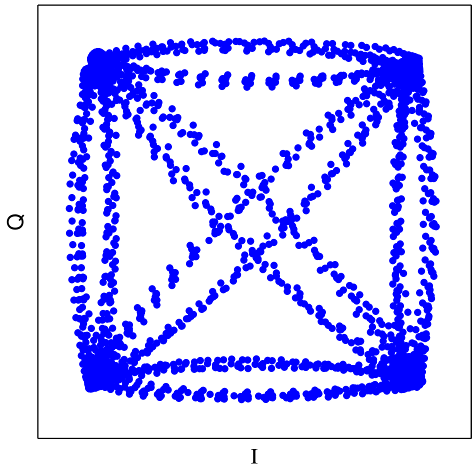

Figure 3.4: QPSK constellation diagram with double rails. The constellation diagram was produced in computer simulations by applying a 18 GHz FWHM Gaussian filter that was not centered around zero frequency. The symbol rate was 10 GBaud and the filter offset was 2 GHz.

rails is shown in Fig. 3.4. Each transition is split up into two rails, each of the rails coming from one of the two possible directions of the transition. The same thing will happen if an optical filter is not centered on the transmitter laser frequency.

The low pass filtering was implemented with several alternative filter transfer functions. The ones focused on were Bessel filters and Gaussian filters. Bessel filters are interesting because they have been used traditionally when testing on-off keyed systems. Gaussian filters were seen as interesting because they are mathematically convenient and well defined and because they have a constant phase response. The transfer function of a Bessel filter is

$$H(\omega) = \frac{\theta_n(0)}{\theta_n(j\omega/\omega_0)} \tag{3.7}$$

where $\theta_n(s)$ is the Bessel polynomial of order n and ω_0 determines the filter bandwidth [15]. The transfer function of a Gaussian filter is

$$H(\omega) = e^{-\omega^2/\omega_0^2} \tag{3.8}$$

where again ω_0 decides the filter bandwidth [16, p. 1125]. It is worth noting that the transfer function of the Gaussian filter is real valued, which may prove to be advantageous when trying to implement an optical filter. The DSP filtering calculations was performed in the same way as described in the beginning of chapter 4.

3.7 Phase estimation for impulse response measurements

This section concerns the impulse response measurements described in section 5.2. Even though the measurements of the impulse response were performed with a self-homodyne system, i.e. by using the same laser as signal and LO, phase tracking was needed. This is due to the optical path length of the pulse and the LO not being matched exactly which led to a phase variation between the pulse and the LO. However it should be noted that the phase which had to be tracked had much smaller variations than in the intradyne experiments with QPSK data. The phase tracking was performed with a simpler algorithm than in the case with QPSK data. The first step was to locate the pulses which was done by finding the spike in the power spectrum, this was done in the same manner as for QPSK signals. The phase of the pulses were found by interpolating their phase at the maximum points. After that the phase of the intermediate

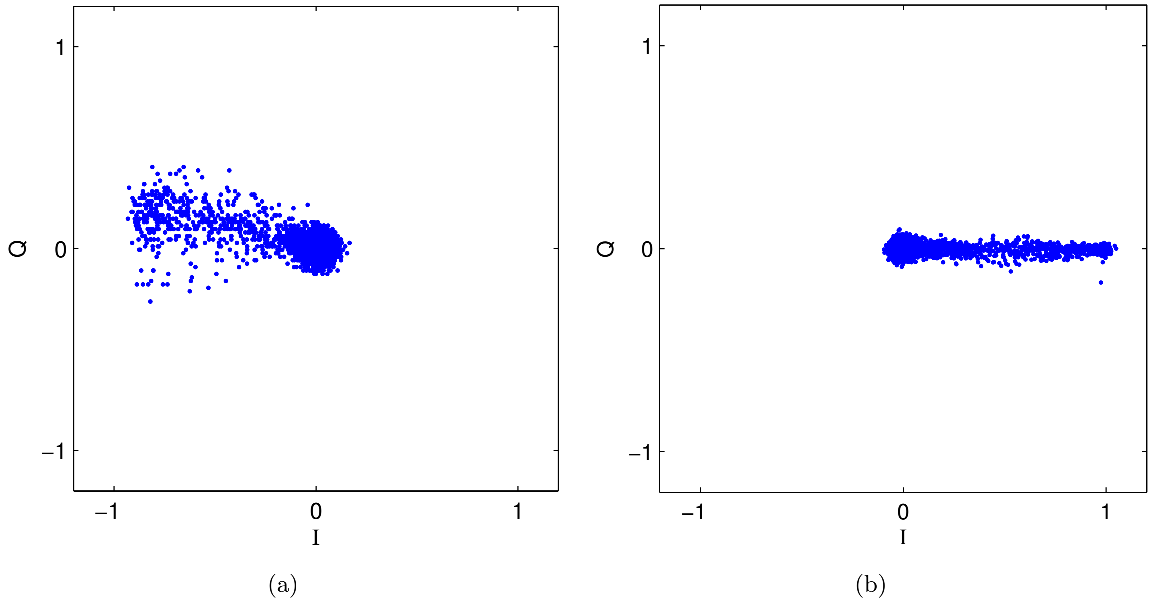

Figure 3.5: Impulse response measurements in the IQ-plane. (a) The measured impulse response before phase tracking. (b) The measured impulse response after phase tracking.

points between pulses was linearly interpolated from the phase at the maximum points. The phase of all data points was corrected so the pulses were aligned with the I-axis.

Plots showing measured impulse responses in the I-Q plane before and after phase estimation is shown in Fig. 3.5. We see that the phase noise is removed so that all pulses have the same phase and are all aligned with the I-axis.

Chapter 4

Optical filtering

Optical filters are used in all kinds of applications for many different purposes. Uses range from improving camera lens performance with optical filter coatings to filtering out certain wavelength channels in a fiber optic network. When selecting a channel with an optical filter in a fiber optic network one ideally wants to filter out the signal unaffected. In this thesis the focus will be on filtering that affects the signal significantly by narrowing the spectrum and possibly applying phase characteristics.

4.1 Theoretical description of an optical filter

An optical filter is completely described by its frequency response, which is information on how the amplitude and phase is affected for each frequency component. This is most often given in the form of a complex valued transfer function $H(\omega)$ such that the amplitude response is given by $|H(\omega)|$ and the phase response by $\arg(H(\omega))$. The output $v(t)$ from the filter is given by $v(t) = \mathcal{F}^{-1}(H(\omega)\mathcal{F}(u(t)))$ where $u(t)$ is the input signal to the filter. The Fourier transform and its inverse are defined as

$$\mathcal{F}(h(t)) = \hat{h}(\omega) = H(\omega) = \int_{-\infty}^{\infty} h(t)\ e^{-j\omega t}\,dt \tag{4.1}$$

and

$$\mathcal{F}^{-1}(H(\omega)) = h(t) = \int_{-\infty}^{\infty} H(\omega)\ e^{j\omega t}\,d\omega. \tag{4.2}$$

Alternatively the filtering can be calculated in the time domain using convolution and thus avoiding Fourier transforming the signal but instead inverse fourier transforming the filter transfer function. The output is then calculated as $v(t) = \mathcal{F}^{-1}(H(\omega)) \otimes u(t)$, where $\otimes$ stands for convolution. The convolution is defined as

$$f(t) \otimes g(t) = \int_{-\infty}^{\infty} f(\tau)\,g(t-\tau)\,d\tau. \tag{4.3}$$

Both methods are equivalent.

4.2 Equivalence between optical and DSP filtering

This section aims at clarifying what the equivalent filter looks like in the DSP domain compared to optical filtering. The next step is to establish if it is possible to achieve the same results by filtering optically as by applying hardware electrical filters on the output ports or digital filtering in DSP. Start by recalling the real-valued expressions for the signal and LO fields.

$$E_s(t) = \frac{1}{2}u(t)(e^{i(\omega_s t+\phi_s(t))} + e^{-i(\omega_s t+\phi_s(t))}) \tag{4.4}$$
$$E_{LO}(t) = \frac{1}{2}v_0(e^{i(\omega_{LO} t+\phi_{LO}(t))} + e^{-i(\omega_{LO} t+\phi_{LO}(t))}) \tag{4.5}$$

Begin with the derivation of the discrete output after the DSP, $r_{k,DSP}$ in the DSP filtered setup shown in Fig. 4.1. The output is calculated as

$$\begin{aligned} r_{k,DSP} &= \mathcal{F}^{-1}\left[H_{DSP}(\omega)\mathcal{F}\left[RE_sE^*_{LO}\right]\right] \\ &= \mathcal{F}^{-1}\left[H_{DSP}(\omega)\mathcal{F}\left[\frac{1}{4}Ru(t)v_0\left(e^{j(\omega_{IF}t+\phi(t))} + e^{-j(\omega_{IF}t+\phi(t))}\right)\right]\right]. \end{aligned} \tag{4.6}$$

Note that the terms with frequency $\pm(\omega_s + \omega_{LO})$ were omitted. By Fourier transforming the whole expression we get the output signal from the system

$$\mathcal{F}[r_{k,DSP}] = \frac{1}{4}RH_{DSP}(\omega)v_0\hat{u}(\omega-\omega_{IF}) \otimes \mathcal{F}\left[e^{j\phi(t)}\right] + \frac{1}{4}RH_{DSP}(\omega)v_0\hat{u}(\omega+\omega_{IF}) \otimes \mathcal{F}\left[e^{-j\phi(t)}\right]. \tag{4.7}$$

Under the assumption that $\omega_{IF} = \phi(t) = 0$ we get the output in the frequency domain to be

$$\mathcal{F}[r_{k,DSP}] = \frac{1}{2}RH_{DSP}(\omega)v_0\hat{u}\left(\omega\right). \tag{4.8}$$

Now, to the optically filtered case described in Fig. 4.2 where the output signal can be written as

$$\begin{aligned} r_{k,opt} &= R\mathcal{F}^{-1}\left[H_{opt}(\omega)\hat{E}_s(\omega)\right]E^*_{LO} \\ &= R\mathcal{F}^{-1}\left[H_{opt}(\omega)\hat{E}_s(\omega)\right]\frac{1}{2}v_0(e^{j(\omega_{LO}t+\phi_{LO}(t))} + e^{-j(\omega_{LO}t+\phi_{LO}(t))}). \end{aligned} \tag{4.9}$$

By fourier transforming and using one of the properties of the Fourier transform, $h(t) = e^{j\omega_0 t}f(t) \Rightarrow \hat{h}(\omega) = \hat{f}(\omega-\omega_0)$, we get

$$\mathcal{F}[r_{k,opt}] = \frac{1}{2}RH_{opt}(\omega-\omega_{LO})v_0\hat{E}_s(\omega-\omega_{LO})\otimes\mathcal{F}[e^{j\phi_{LO}(t)}] + \frac{1}{2}RH_{opt}(\omega+\omega_{LO})v_0\hat{E}_s(\omega+\omega_{LO})\otimes\mathcal{F}[e^{-j\phi_{LO}(t)}]. \tag{4.10}$$

The next step is to rewrite $\hat{E}_s(\omega-\omega_{LO})$ and $\hat{E}_s(\omega+\omega_{LO})$ on the form

$$\begin{aligned} \hat{E}_s(\omega-\omega_{LO}) &= \mathcal{F}\left[E_s(t)e^{j\omega_{LO}t}\right] = \frac{1}{2}\hat{u}(\omega-\omega_{IF}) \otimes \mathcal{F}\left[e^{-j\phi_s(t)}\right], \\ \hat{E}_s(\omega+\omega_{LO}) &= \mathcal{F}\left[E_s(t)e^{-j\omega_{LO}t}\right] = \frac{1}{2}\hat{u}(\omega+\omega_{IF}) \otimes \mathcal{F}\left[e^{j\phi_s(t)}\right]. \end{aligned} \tag{4.11}$$

Inserting this into equation 4.10 and again omitting terms at frequencies $\pm(\omega_s + \omega_{LO})$ yields

$$\mathcal{F}[r_{k,opt}] = \frac{1}{4}RH_{opt}(\omega-\omega_{LO})v_0\hat{u}(\omega-\omega_{IF})\otimes\mathcal{F}\left[e^{j\phi(t)}\right] + \frac{1}{4}RH_{opt}(\omega+\omega_{LO})v_0\hat{u}(\omega+\omega_{IF})\otimes\mathcal{F}\left[e^{-j\phi(t)}\right]. \tag{4.12}$$

We now see that equality between $r_{k,opt}$ in equation 4.12 and $r_{k,DSP}$ in equation 4.7 requires that

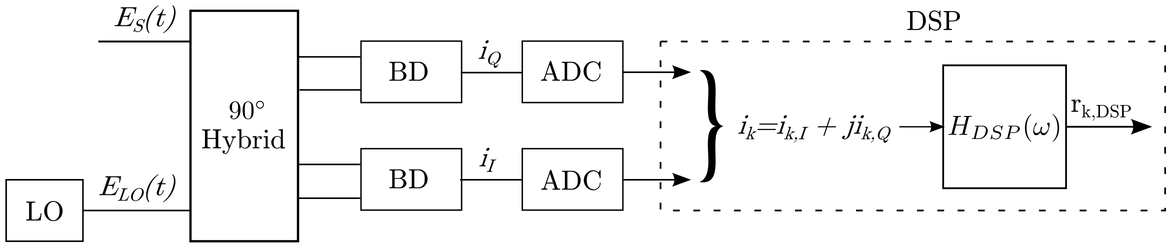

Figure 4.1: Schematic of the electrically filtered setup, BD is short for balanced detector and ADC for analog-to-digital converter.

$$H_{opt}(\omega) = H_{DSP}(\omega \pm \omega_{LO}). \tag{4.13}$$

The reason for the $\pm$ in equation 4.13 is that the fourier transform of $\sin(\omega t)$ has components at both $\pm\omega$. This is purely mathematical and does not mean that there is a signal at negative frequencies. Again we see that by setting $\omega_{IF} = \phi(t) = 0$ we get the output in the frequency domain to be

$$\mathcal{F}[r_{k,opt}] = \frac{1}{4} R v_0 \hat{u}(\omega) \left(H_{opt}(\omega - \omega_{LO}) + H_{opt}(\omega + \omega_{LO}) \right) = \frac{1}{2} R H_{DSP}(\omega) v_0 \hat{u}(\omega). \tag{4.14}$$

This proves that under the conditions assumed it is equivalent to filter the signal optically and to filter the complex representation of the field in DSP after IF and carrier phase tracking assuming that the filter transfer functions obey equation 4.13. The derivation also assumes that the sampling rate and bandwidth of the ADC is high enough so that the field is sampled perfectly. The transfer function of the ADC might also have to be taken into account, when and why is discussed in the next section.

Another thing which have to be considered is where the noise sources are compared to where the filtering happens. Consider for example, thermal noise in the ADC which has a different impact depending on where the filtering takes place. If the signal is optically filtered, the noise in the ADC is detected over the whole ADC bandwidth. On the other hand, if the signal is filtered in DSP, part of the noise will be filtered out. This is a real effect, however it does not seem to affect the measurements that was done to a high degree since the noise levels of both the electrically and optically filtered setup was similar.

It should also be pointed out that the optical filtering approach requires that the optical filter can be centered at the frequency of the signal laser with good accuracy. In the experiments which were performed at 10 GBaud, the accuracy of the optical filter center frequency was 1 GHz. The errors due to this did not affect the measurements visibly. The errors due to misaligned center frequency will be even smaller at higher symbol rates. This has to be taken into account, but in most cases it will not cause problems.

4.3 Alternative filtering approaches

There are at least two alternative ways of filtering the signal in addition to the ones described in 4.2. The first and least complex is to insert hardware electric low-pass filters between the balanced detectors and ADC in Fig. 4.1. This is not possible when using optical sampling since there is no electrical real-time output to filter. Another downside of using this approach is that the filtering will cause problems if the intermediate frequency is too large. This would cause the signal spectrum to be filtered asymmetrically and thus generating double rails in the

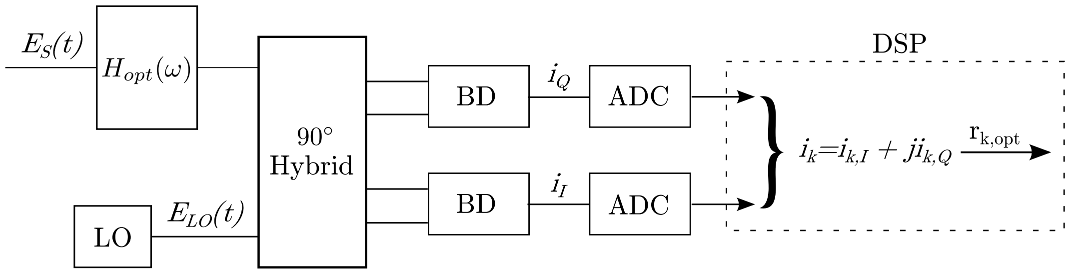

Figure 4.2: Schematic of the optically filtered setup, BD is short for balanced detector and ADC for analog-to-digital converter.

constellation diagram. Also, the transfer function of a hardware electric filter is fixed and not programmable. Thus, hardware electrical filters is not a good filtering approach.

The possibility of a second approach opens up when using optical sampling. It is also possible to put the optical filter between the LO pulse source and the 90° hybrid. This will have the same impact on the output signal as the optical filtering shown in 4.2. Such filtering has not been investigated in further detail. The advantage of this approach is that the insertion loss on the signal input due to the optical filter could be avoided. Also it could be easier to center the optical filter at the LO frequency. This is since the spike in the CW LO frequency spectrum is narrow and very distinct. It would be easier to center the optical filter on a narrow spike than on a wider signal spectrum. This requires that the pulsing of the LO can be turned off so that it emits CW light.

The compatibility between different approaches to filtering and sampling is shown in table 4.1. The only filtering technique that is compatible with all sampling technologies is optical filtering. The only sampling technology that is compatible with all filtering techniques is real-time electrical sampling.

4.4 ADC transfer function

In the previous calculations the transfer function of the ADC was considered to be completely flat, not affecting the signal at all. This is not true. In fact the transfer function of the ADC is more similar to a brick-wall characteristic with a flat top and sharp roll off. The reason why the transfer function of the ADC was ignored is that the oscilloscope used as ADC in the experiments had a bandwidth about twice as high as the bandwidth of the used filters. The oscilloscope had a specified bandwidth of 20 GHz and the signal transmitted in the experiments was QPSK at 10 GBaud, this corresponds to a bandwidth of approximately 10 GHz. Within the signal bandwidth, the oscilloscope transfer function was considered ideally flat and thus was not taken into account.

Using optical undersampling eases the requirements on the ADC bandwidth and sampling rate. If the signal is optically sampled at 1 GHz sampling rate, it is sufficient to have an ADC with a bandwidth and sampling rate of approximately 1 GHz. Still the measurement bandwidth of the optical sampling system could be much higher.

4.5 Candidate optical filters

There are numerous ways to construct optical filters. A lot of work was spent on investigating which of these filters that were suitable to use in the project. Desirable filter properties are wavelength tunability, ability to emulate transfer function of an electrical filter, low insertion

Table 4.1: Table showing which sampling technologies that are compatible with different filtering technologies, Y marks compatibility.

Filtering \ Sampling	El. real-time	El. undersampling	Opt. real-time	Opt. undersampling
DSP filtering	Y	N	Y	N
HW El. filtering	Y	Y	N	N
Opt. filtering	Y	Y	Y	Y

loss and low complexity/price. Wavelength tunability is wanted because a test rig must be able to test at different wavelength channels. Ability to emulate any given transfer function is not a must in an actual testing rig but for this investigative study it is considered essential. Filters that were investigated were thin-film, Mach-Zehnder, grating, acousto-optic, arrayed waveguide grating (AWG), and programmable filters based on liquid crystal on silicon technology, LCoS. Only the filters that were considered interesting are covered to some extent in the thesis.

Thin-film and grating filters lack wavelength tunability. Mach-Zehnder and acousto-optic filters are tunable but can not emulate any given filter transfer function. This leaves LCoS-based filters, which are both tunable and can at least in theory emulate any given transfer function. Also worth mentioning are AWG:s, which are appealing because of low cost and because they are designed such that they can filter out any of the channels of the C-band used in fiber optics.

4.5.1 LCoS programmable filters - Finisar Waveshaper

Liquid Crystal on Silicon (LCoS) based filters currently represent the most versatile optical filtering technology. The center frequency of the filter is tunable and the phase and amplitude response of the transfer function can be chosen arbitrarily. The filter used in the experiments was a Finisar Waveshaper 1000E that has an insertion loss of 4.5 dB, which was acceptable [17]. The biggest drawback of the Waveshaper is the price. It cannot be considered a low cost alternative. Articles with overviews of how the technology works, and examples of other applications, can be found in the references [18] [19].

The Waveshaper can in theory be used to emulate any filter characteristic such as Gaussian, Bessel, Butterworth or Chebyshev. However, there are practical limitations to which filters it can generate. The experiments indicate a slight wavelength dependence of the filter transfer function for narrow filters. It also seems that the shape of the transfer function is incorrect for very narrow filters. The parameter which affected the accuracy of the attained optical filter most was whether the filter had a non-constant phase response. Using a constant filter phase response greatly improved the accuracy of the amplitude response. Because of the problems with filters which have rapidly changing phase responses, all filters which were used in the experiments had constant phase.

Examples of the accuracy of the attained optical filter from the Finisar Waveshaper is illustrated in Fig. 4.3. The measurement of the filter shapes was done by feeding amplified spontaneous emission (ASE) noise from an EDFA into the filter and measuring the output spectrum with a optical spectrum analyzer (OSA). It should again be pointed out that this gives no information on the accuracy of the filters phase response. When comparing the accuracy of the gaussian filter to the accuracy of the Bessel filter it is clear that the gaussian filter has better consistency with the ideal filter shape. The worse accuracy of the Bessel filter in Fig. 4.3(b) can be explained by the phase response of a Bessel filter which is rapidly changing which seems to cause problems with the Waveshaper. The gaussian filter in Fig. 4.3(a) on the other hand has a constant phase response which seem to result in excellent accuracy of the amplitude response.

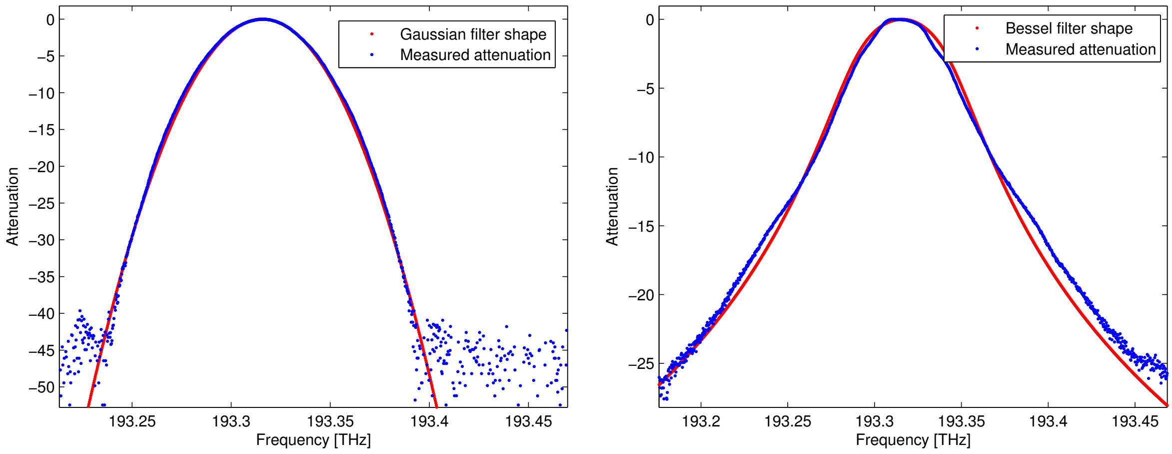

(a) (b)

Figure 4.3: Accuracy measurements for the optical filters attained with the Waveshaper. In the plots are both the measured and ideal filter characteristics plotted. The FWHM of the filters was 42 GHz. (a) shows the results for a Gaussian filter and (b) shows the results for a Bessel filter with non-constant phase response. Notice that the accuracy is worse for filters with rapidly changing phase response.

4.5.2 Thin-film filters

Thin-film filters or interference filters are made by stacking layers of materials with different refractive index. The reflected and transmitted field interfere at the interfaces between layers to generate the amplitude and phase response of the filter. It is possible to generate a filter with arbitrary transfer function by choosing appropriate thickness and refractive index of the layers. For a vivid example of this, one can read about Dobrowolski´s filter with a transfer function shaped like the Taj-Mahal [20]. Modern computer programs exist capable of generating a filter design starting from a specified arbitrary transfer function [21].

The downside of thin film filters is that they are not wavelength tunable, a given design will have a fixed center wavelength and transfer function. Since modern fiber optic communication systems work at up to 100 different wavelengths they are not viable options to use for signal characterization.

4.5.3 Arrayed waveguide grating

Another alternative is to use so called AWG:s. These devices are normally used to separate the optical signals at different wavelengths and output them to different optical fibers at the receiver side or, inversely at the transmitter, to multiplex several optical signals at different wavelengths onto the same optical fiber. AWG:s are designed to multiplex and demultiplex signals according to the frequencies defined by the standardized DWDM ITU-grid [22].

The transfer function of an AWG has a pass-band characteristic with a constant phase response [23]. This makes them unusable in order to emulate an electric filter. They can only be used to bandwidth limit the signal. The advantages of using AWG:s are many, they can be accurately emulated in DSP, they are cost effective and clearly defined in standards. The transfer function of an AWG is modelled well with a supergaussian function. All of these points make a strong case for using AWG:s in a standard based on optical filtering. In this project, we did not have the possibility of performing experiments with an AWG.

Chapter 5

Experiments and simulations

The purpose of the experiments is to determine whether the optical filtering is accurate enough compared with filtering in DSP and to prove that it is possible to develop a standard for signal quality characterization based on optical filtering. The experiments were designed to offer direct comparisons between optically filtered results and DSP filtered results. The computer simulated system will be presented after the experimental setups.

5.1 Experimental setup for measurements on QPSK signals

The purpose of the experiments with QPSK-modulated signals was to study the effect of the different ways of filtering. The retrieved signal is then used to generate TR-EVM plots which will be shown in chapter 6 to compare the different cases.

When performing the experiments, a so called OIF (Optical Internetworking Forum) receiver was used. This is an integrated unit with 90° hybrid and balanced photo detectors in one package. OIF is an international standardizing organisation. The OIF receiver was a u^{2}t photonics CPDV1200R. The programmable optical filter was a Finisar Waveshaper 1000E. The oscilloscope used as ADC was a LeCroy SDA 820Zi-A that had a 20 GHz electrical bandwidth and 40 GS/s sampling rate. The frequency of the LO and signal laser was 193.3 THz. All experiments were performed back-to-back with signal in one polarization. The schematic is shown in Fig. 5.1.

The system uses intradyne reception. This means that the LO and signal laser are close in frequency, the intermediate frequency ω_{IF} was on the order of 1 GHz. The overall design of the system is typical [8].

To study the unfiltered case, the Waveshaper was simply set to the transmit state where all light passed straight through. This way the same setup could be used to study both an electrically and an optically filtered signal.

It should be noted that the generated signal had very fast transitions between symbols and as a result, a very high bandwidth. This is because the PRBS and IQ-modulator were made for higher symbol rates while it was only being used at 10 GBaud. The OIF receiver was also made for higher symbol rates, it was specified to handle up to 64 GBaud. This means that the bandwidth-limiting component with no filters applied was the ADC. With filters applied, the ADC bandwidth was high enough so that the ADC would not bandwidth limit the signal.

Noise should not be a big concern in these experiments. There is no amplification of the optical signal which could be a potential noise source. There are however electrical amplifiers before the IQ-modulator which could add some noise on the IQ-channels. Another noise source is thermal noise in the receiver, the implications of this were discussed in the end of section 4.2. If the transmitted data is periodic and of known length, it is possible to average out the noise by collecting measurements from several consecutive measurements. The noise levels in the experiments were considered very low since the experiments were performed in close to ideal

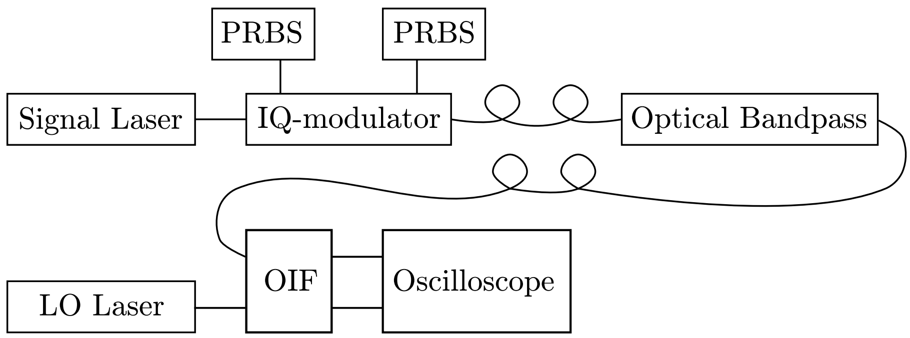

Figure 5.1: The experimental setup for measurements on QPSK signals.

conditions, i.e. back-to-back and without optical amplification.

5.2 Experimental setup for impulse response measurements

The purpose for doing impulse response measurements was to have one measurement which took the frequency characteristic of the whole system into account. Assuming that the measured impulse response is correct it can also be used in order to numerically calculate the output from the system given any arbitrary input signal. In this project however, the impulse responses were used to do comparison between the DSP filtered and optically filtered setups.

The impulse response measurements were performed with homodyne detection, this means that the signal laser was split by a 3-dB coupler and one of the outputs was used as LO. The CW light from the other output was shaped into 16 ps FWHM pulses by a pulse carver driven by microwave electronics. The experimental setup is shown in Fig. 5.2.

The initial assumption was that no phase tracking would be needed for these measurements. This turned out to be incorrect due to the difference in optical path length of the LO and pulse path. In total the pulse source had approximately 20 m of optical fiber, the length of that optical fiber could not be matched with sufficient accuracy to the LO optical path length. Worth mentioning is that the linewidth of the laser strongly affects the tolerances on the optical path lengths and how much phase noise there will be in the homodyne system. A narrower linewidth will allow for bigger differences in optical path length. The laser that was used in the experiments had a linewidth specified at maximum 100 kHz.

Attempts were made to shorten the pulses further by applying sinusoidal phase modulation and letting the pulse travel through a dispersive fiber. This approach did not give any useful results, the reasons for this was not fully understood. Possible explanations are that the pulse still had residual chirp after the fiber or that the differing characteristics of the I and Q channel caused problems. After trying this we settled for pulses which could be achieved only by pulse carving, the shortest possible pulses had a FWHM of 16 ps and a bandwidth of 64 GHz FWHM. The pulse bandwidth is more than three times wider than the applied 18 GHz filters. The pulses had a repetition rate of 1 GHz which led to a duty cycle $D = 16\text{ps}/1\text{ns} = 0.016$. The electric pulses were generated by feeding two 1 GHz square waves into a logic AND circuit with a slight delay on one input. The AND circuit would then give an output only during the short offset and thus generate pulses.

To find the impulse response, measurements over many pulses were used. The samples were gathered into bins according to their position over the duty cycle. The bins represent time intervals at different positions in the duty cycle. Then the average of the samples in each bin was calculated to average out the noise and find the waveform. This was done after the phase tracking described in section 3.7. For the plots presented in chapter 6, averaging was done over

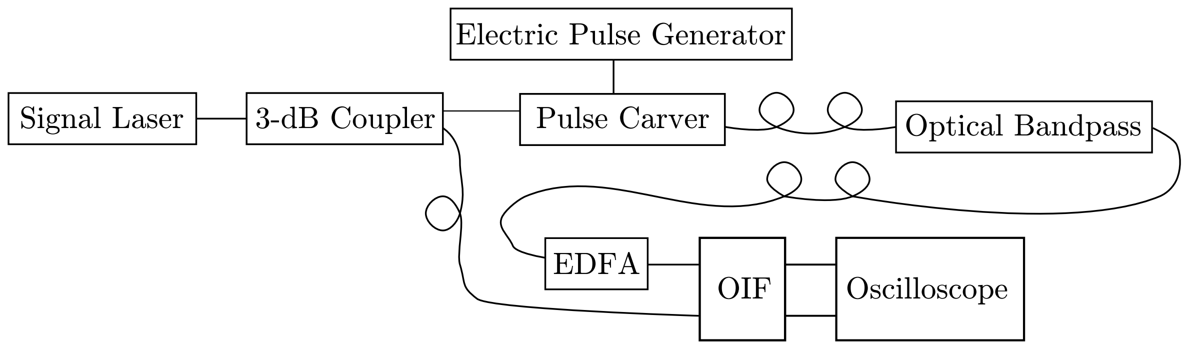

Figure 5.2: The experimental system used for measurements of impulse responses.

approximately 2500 pulses.

A problem in the experimental setup is that there was timing mismatch between the I- and Q-channel, up to 20 ps. This problem probably came from the electrical connectors between hybrid and oscilloscope or the hybrid itself. The result of small timing errors is that the detected pulses will be shaped like a loop instead of a straight line in the I-Q plane at phase angles around 45°, 135°, 225° and 315°. The reason for this being that at those angles there is output from both the I and Q channels. This was corrected manually, either by tuning time delay in the oscilloscope or in DSP.

The power loss in the optical pulse path also turned out to be a problem. The signal power at the receiver was not high enough and to correct this problem, an EDFA was used before the receiver in order to reach sufficient input power. Because of the averaging used to retrieve the waveform of the pulses, the noise added by the EDFA should not affect the quality of the measured impulse response.

5.3 Computer simulated system

Computer simulations were performed in order to test different filters and to see how they affected the TR-EVM, constellation diagram, eye diagrams, and signal spectrum. Simulations were compared to experimental results to see how close the experimental results are to the ideal computer simulated results. For measurements at higher symbol rates, i.e. 28 Gbaud, it was not possible to filter the signal in DSP since the signal was detected with undersampling with the PSO-200 optical modulation analyzer. Thus the only comparison and confirmation of the results that could be made for higher symbol rates was with computer simulations.

The parts of the simulated fiber optic communication system are shown in Fig. 5.3. The first step is generation of the electric signals driving the I-Q modulator. The electric signals were generated as raised cosine envelopes modulated with pseudorandom binary sequence (PRBS) data. The I and Q signals were then fed into a linear I-Q modulator to get the electric field of the optical signal. Filtering of the optical signal was performed in the frequency domain. The receiver was ideal and e.g. timing skew or imbalance between I- and Q-channels was not modelled. All simulations were performed with the signal centered at zero frequency.

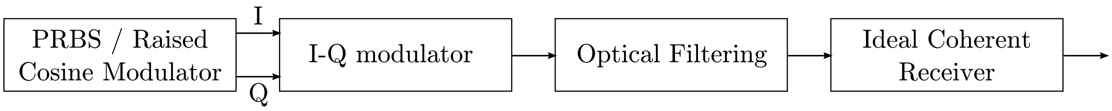

Figure 5.3: Overview of the computer simulated system.

Chapter 6

Results

The results from the experiments will be presented in this chapter. There are three sections, the first with results from the measurements on QPSK data and the second section with impulse response measurements. The third section contains data from measurements on faulty signals. The measurements on QPSK data will also be compared to computer simulations, which will be used as a reference. The results from both the QPSK measurements and the impulse response measurements will be used to confirm that the optically filtered setup is a viable option to use for signal quality characterization.

6.1 TR-EVM comparisons

This section is dedicated to comparisons of TR-EVM measurements with the signal unfiltered, filtered optically and filtered in DSP. The experimental setups are shown in Figs. 4.2 and 4.1. Computer simulated TR-EVM plots are used as a reference which shows the ideal case. The reason for doing this comparison is to establish that the Waveshaper can emulate the chosen filter functions with sufficient precision and to show experimentally what was proven theoretically in section 4.2. The results of the TR-EVM measurements are shown in Fig. 6.1. The transmitted signal was modulated with QPSK at 10 GBaud. The transmitted data was a PRBS pattern with a length of 508 symbols, $4(2^7 - 1)$.

The unfiltered signal in Fig. 6.1(a) is bandwidth limited by the oscilloscope, this is the reason behind the ringings in the flat region in the middle of the TR-EVM plot. This comes from the lost signal energy outside the flat region of the oscilloscope response. The power spectrum of the 10 GBaud QPSK signal and the oscilloscope bandwidth is shown in Fig. 6.2. Also note that these ringings seem to lead to a slight increase of the EVM in the middle of the symbol slot compared to filtered measurements. The EVM of the DSP filtered signal is lower than the EVM of the optically filtered signal. This is probably because the DSP filter also removes some thermal noise from the receiver and ADC. The ideal case is represented by the computer simulated plot in Fig. 6.1(b) which is sort of a reference to compare the experimental results in Fig. 6.1(c) and 6.1(d) to. The most important result of these measurements is the striking similarity between the optically filtered TR-EVM measurements and the measurements which were filtered in DSP. This is a first hint towards which optical filters that could be used in an optically filtered system used for signal characterization.

The next step is to quantify the observed similarity between the optically and DSP filtered TR-EVM plots in Fig. 6.1. This was done by calculating the TR-EVM$_{ref}$ using the waveforms from the two measurements. The waveforms of the signals were found by averaging over consecutive PRBS patterns. After finding the waveform of the pattern by averaging the two differently filtered waveforms had to be aligned in time. The Q-part of the waveforms from a small section of the data pattern is shown in Fig. 6.3(a) to illustrate the difference between the waveforms. Then the TR-EVM$_{ref}$ was calculated using one of the averaged waveforms as reference. An explanation of how this is done is found in section 2.5.3. The resulting TR-EVM$_{ref}$ plot is shown in Fig. 6.3(b). As can be seen, the distribution of the data points around the center of the bit slot is reasonably symmetric. The difference between the optically filtered waveform and the DSP filtered waveform is largest in the transitions between symbol slots. A problematic result here would have been if the data points had high values and a highly asymmetrical distribution as this would mean that one of the filters had a non-constant phase response. If the two waveforms were perfectly identical, all samples would have zero-value.

All filters used in these experiments had a constant phase response, i.e. the filters transfer function was real-valued. The reason for this being the inaccuracy of the Waveshaper when programmed with filters with rapidly changing phase response, such as Bessel filters, which was illustrated in Fig. 4.3. When using constant phase filters the accuracy of the Waveshaper seems to be good.

The reason for using a FWHM filter bandwidth of 18 GHz is that the Waveshaper had troubles when trying to produce narrower filters. It was possible to produce narrower filters but this seemed to induce chirp on the signal. At approximately 18 GHz FWHM bandwidth the Waveshaper produced reliable constant phase Bessel filters. Had it been possible, it would have been interesting to use even narrower filters which would have had even greater impact on the signal and the effects of the filtering would have been made more clear.

6.2 Impulse response measurements

This section will be dedicated to presenting the results of the impulse response measurements done with the setup described in section 5.2. That section also describes the involved DSP and the homodyne detection in more detail. These measurements were performed in order to find the complete frequency response, including the ADC. In addition to the measurements of the impulse responses, a more accurate measurement of the input optical pulse was performed. The measured impulse responses are plotted in Fig. 6.4. The input optical pulse had a pulse length of 16 ps and is shown in Fig. 6.5. It was measured with a PSO-100 optical sampling oscilloscope, which has a significantly higher bandwidth (500 GHz FWHM) compared to the coherent detection system, which is limited by the oscilloscope electrical bandwidth at 20 GHz. This can be seen by comparing the width of the unfiltered impulse response in Fig. 6.4 with the width of the input optical pulse in Fig. 6.5. The input optical pulse has about half the width of the unfiltered impulse response. The PSO-100 has sufficient bandwidth to give a realistic representation of the optical pulse. However it should be noted that it measures the intensity of the pulses. The field was approximated by taking the square root of the intensity, which does not give any information on the phase. As an example, it is likely that the small bump just after the pulse has inverted phase relative to the pulse itself, something that cannot be seen in the plot.

The slight bump located at approximately 775 ps in Fig. 6.4 should not be a part of the impulse response, but is an effect of the non-ideal input pulses that have a similar bump at the same time as seen in Fig. 6.5. The source of these bumps were not investigated in more detail. One possible explanation for them is electrical reflections between components in the pulse source. This is likely because the time between pulse and bump corresponds to a microwave cavity of about 4 cm and several connections and components had similar dimensions.

There are ringings on all impulse responses to varying degree. They are most visible on the unfiltered impulse response but are also there in the filtered measurements. The ringings on the impulse responses are the same as those seen affecting the EVM in Fig. 6.1(a). Most likely, they come from the bandwidth limitation of the ADC since the frequency of the ringings is approximately 20 GHz, the same as the oscilloscope electrical bandwidth.

Only the real part of the impulse responses is plotted, no significant information is lost since the imaginary part of the impulse responses was negligible after averaging in all cases.

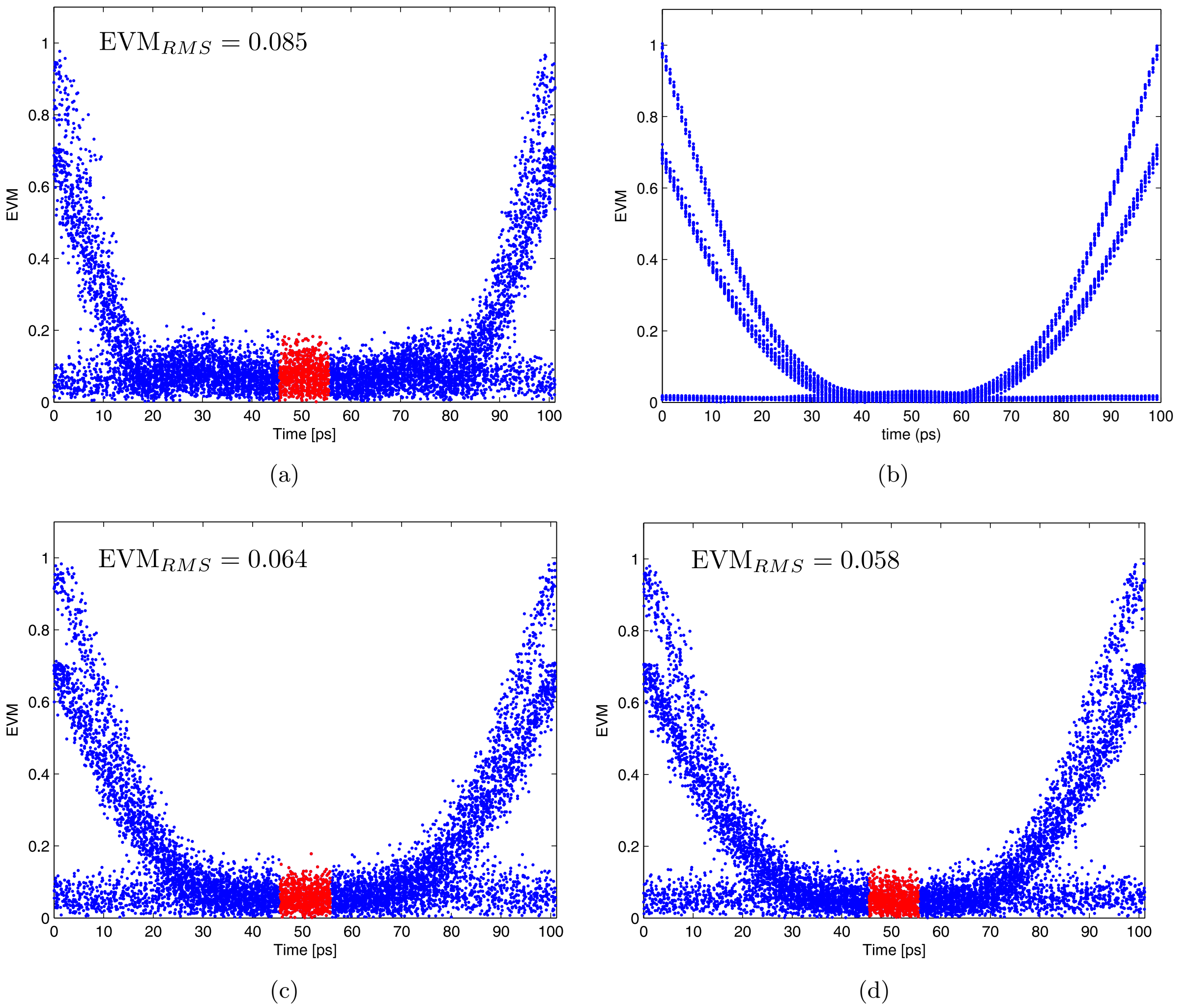

Figure 6.1: TR-EVM measurements on 10 GBaud QPSK signals and simulations. The EVM$_{RMS}$ of the red marked samples has been estimated. Filter bandwidths are given as FWHM. (a) Measurement of unfiltered signal. In this case the oscilloscope is limiting the bandwidth at 20 GHz electrical bandwidth. (b) Computer simulated results, signal filtered with 18 GHz constant phase Bessel filter. (c) Signal filtered optically with waveshaper programmed with a 18 GHz constant phase Bessel filter. (d) Signal filtered with a 18 GHz constant phase Bessel filter in DSP after IF and phase tracking.

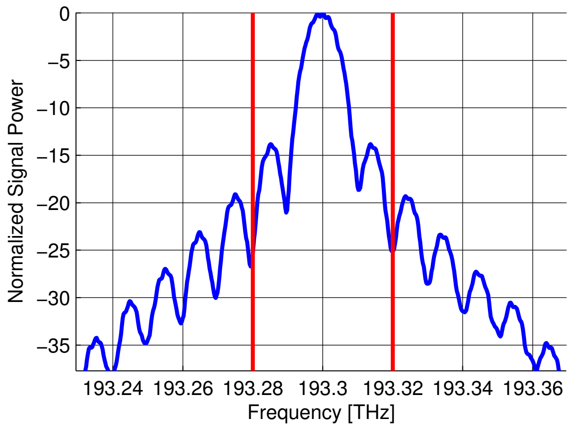

Figure 6.2: The power spectrum of the 10 GBaud QPSK signal. The oscilloscope bandwidth is marked with red lines.

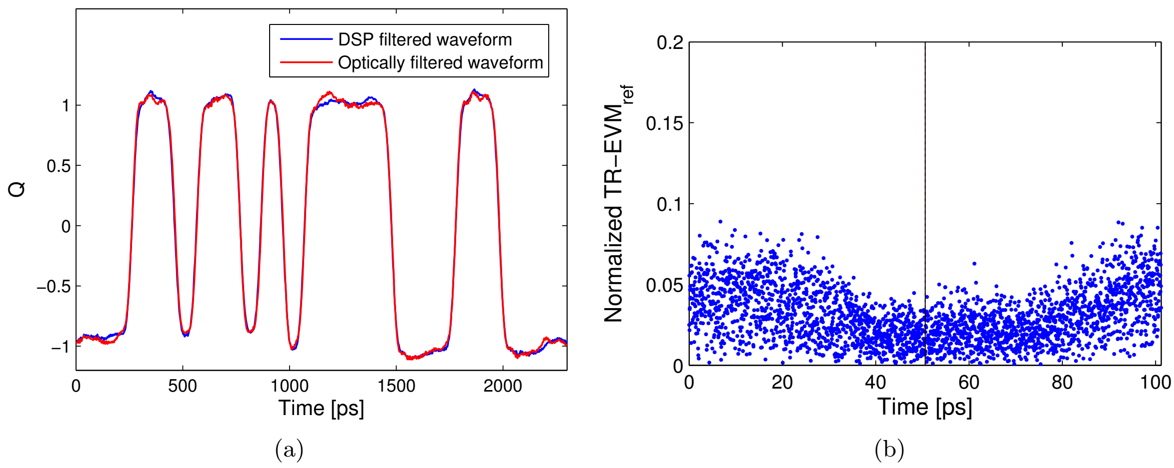

Figure 6.3: (a) The quadrature phase of the optically and DSP filtered waveforms in a 20 symbols long section of the PRBS pattern. The waveforms were found by averaging the signal over consecutive PRBS patterns. (b) TR-EVM$_{ref}$ calculated by comparing the optically and DSP filtered waveforms. The data is from the same measurements that was used for Figs. 6.1(c) and 6.1(d). The signal was modulated with 10 GBaud QPSK data. The center of the symbol slot is marked with a vertical line.

The purpose behind doing the impulse response measurements was to determine if the optically filtered and DSP filtered systems had the same impulse response. As is seen in the figures, the impulse responses are almost identical in the center part where the amplitude is high. In between pulses there is visible ringing and the amount of ringing is not identical for the optical and DSP filtered impulse responses. The reason for this is not fully understood, it could come from inaccuracy of the optical filter far away from the center frequency where the attenuation should be very high. As can be seen in Fig. 4.3(a) there are regions where the attenuation is slightly off for the Waveshaper programmed with a Gaussian filter.

6.3 EVM measurements with signal impairments

Measurements at 28 GBaud were also made. At this symbol rate it was not possible to detect the signal in real-time. This is because the bandwidth of the oscilloscope was too low. To detect these signals, the PSO-200 Optical Modulation Analyzer (OMA) from EXFO was used. The purpose of the measurements was to see how optical filtering affected the EVM with faulty signals. Two different signal impairments were tested. The first tested error was the amount of timing skew between the I and Q channel, i.e. having the I and Q channel of the transmitter misaligned in time. The second tested error was amount of quadrature error, i.e. having the delay in the IQ-modulator different than 90°. The effect of this is that the angle between the I and Q axis will differ from 90°. This can be seen in the QPSK constellation diagram that will be rhombus shaped. The effects of these signal impairments on the TR-EVM are illustrated in Fig. 6.6.

The results of these EVM measurements are shown in Fig. 6.7. The inset pictures show constellation diagrams to illustrate the different errors. As expected, the filtering affects the EVM measurements greatly. Two effects of the filtering are seen. The first effect is that the minimum EVM level is higher for the filtered signals, i.e. the filtering increases the EVM even for ideal signals due to ISI. The other effect is that the increase in EVM due to impairments become visible even for lesser amounts of error and that the slope of the curve is greater.

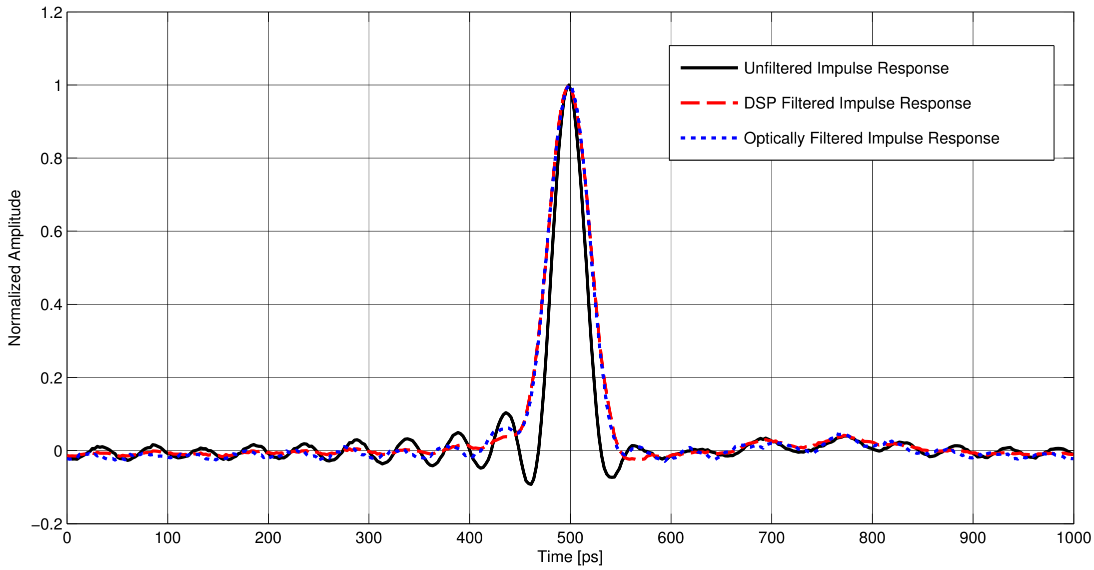

Figure 6.4: Measured impulse responses of the described system, the real part of the field is plotted. Both the optically filtered and the DSP filtered impulse responses have been filtered with a 18 GHz FWHM constant phase Bessel filter.

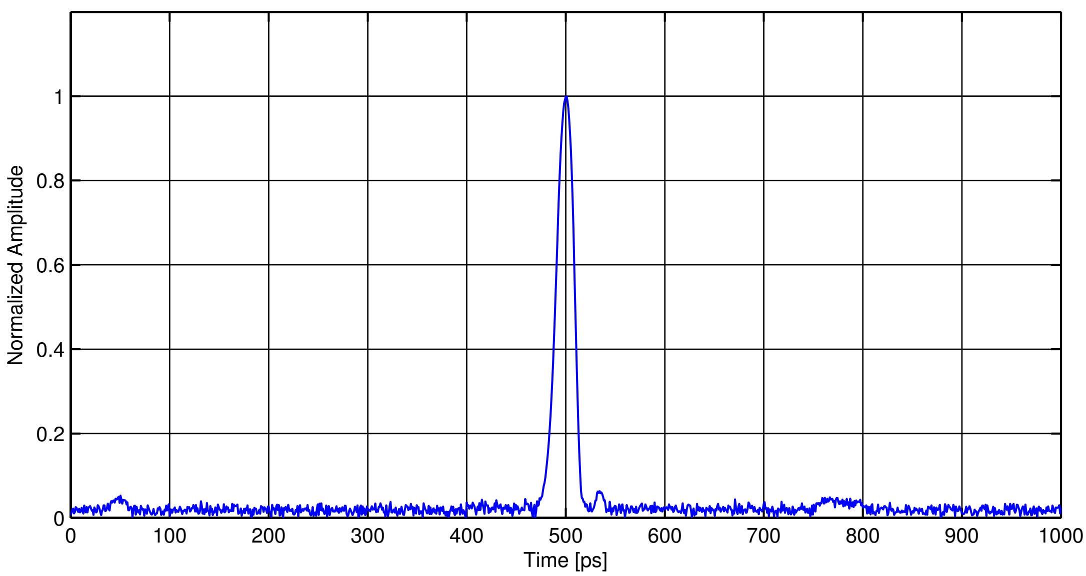

Figure 6.5: The field of the input optical pulse measured with a PSO-100 optical sampling oscilloscope. The FWHM of the pulse is 16 ps.

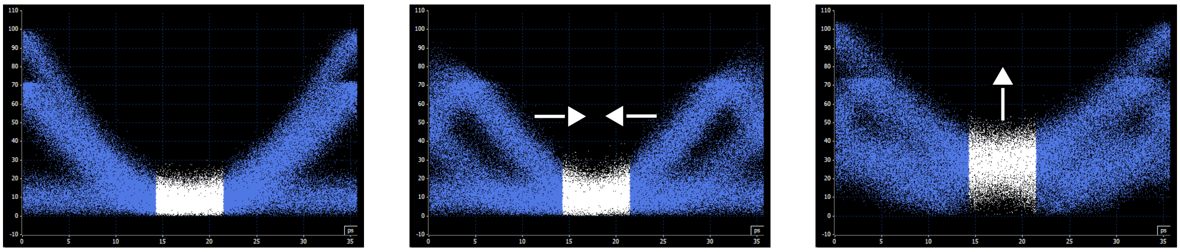

(a) (b) (c)

Figure 6.6: Illustrations of how some different signal impairments affect the EVM and TR-EVM when combined with optical filtering. The measured signal is 28 GBaud QPSK. The applied optical filter is a 28 GHz FWHM Gaussian filter. (a) The ideal signal. (b) 8 ps timing skew between I- and Q-channels. (c) 30° quadrature error.

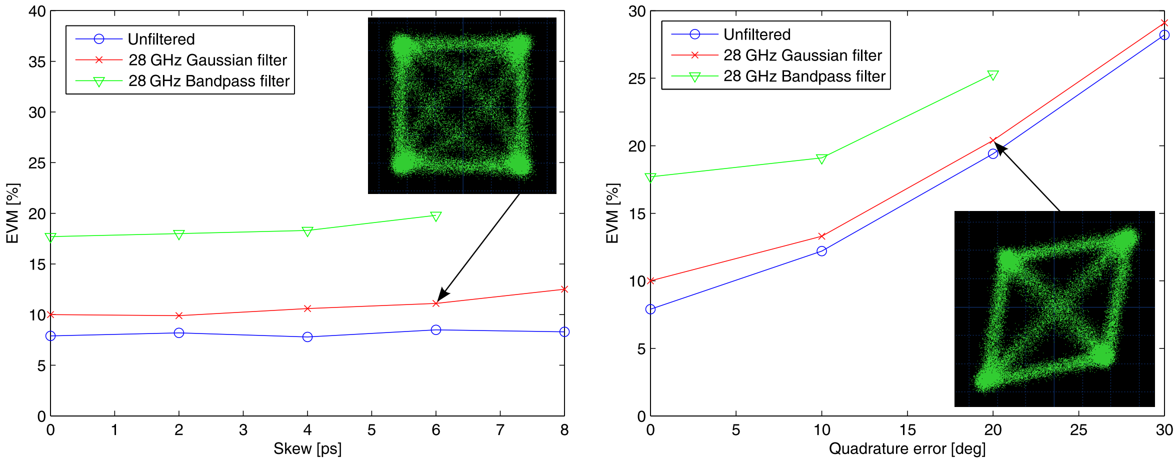

(a) (b)

Figure 6.7: EVM measurements with faulty signals at 28 GBaud. Signals are filtered optically with the waveshaper. The filter characteristics are specified in the legend, filter bandwidths are given as FWHM. The last data points for the band pass filtered measurements are missing since the phase tracking did not function for such narrowly filtered signals with big signal impairments. The inset pictures show the constellation diagram at chosen data points. (a) EVM as a function of timing skew. (b) EVM as a function of quadrature error.

Chapter 7

Conclusions

The conclusions can be divided into three topics. The first is the discussion if optical filtering together with optical sampling is a possible solution from a hardware point of view. The next step is to draw conclusions on the methods that could be used for signal characterization. The last step is to discuss interesting further studies on the subject.

7.1 Test setup

The overall objective of the thesis was to determine if optical filtering is a good approach to filtering for purposes of signal quality characterization. It has been established that it is possible to use optical filters to band pass filter the signal with accuracy comparable to DSP filtering. Depending on the choice of optical filter hardware the choices of filter characteristics can be limited. This study focused on the use of the Finisar Waveshaper for optical filtering. There are limitations to the filter characteristics the Waveshaper can produce. Filtering would be limited to filter characteristics with constant phase and sufficient bandwidth. The constant phase requirement excludes the use of electrical filter characteristics like Bessel, Chebyshev or Butterworth. Bessel characteristics has been used historically when testing OOK systems. Instead, possible filter characteristics include e.g. Gaussian, Bandpass or Super-Gaussian, all of these have constant phase response. The Waveshaper can generate accurate filters with a bandwidth above approximately 20 GHz FWHM. This does not pose a problem when measuring on 28 GBaud QPSK signals which is the data rate of interest at the moment. The filters which would be used for signal characterization of 28 GBaud QPSK would probably have bandwidths of at least 28 GHz FWHM. An advantage of using optical filtering is that it is neutral in terms of sampling technology. Optical filtering is compatible with both electrical and optical sampling.

7.2 Testing methodology

Many different methods for characterizing optical signal quality were discussed in the thesis. All methods have their strengths and weaknesses, the least complex measure is EVM and the most complete picture is given by TR-EVM. Both methods can be used together with filtering. There are several approaches to using filtering together with EVM or TR-EVM.

Very narrow filtering together with EVM measurements is one approach. Due to the narrow filtering, the signal impairments in the transitions between symbols would affect the EVM in the middle of the bit slot. This way, all signal impairments are transformed into one value. A strongly filtered EVM measurement can say that something is wrong with the signal. However, it can be difficult to say, what is wrong with the signal. It is difficult to separate the different errors. This approach was difficult to implement with optical filtering since a very steep filter roll-off is needed. Preferably a perfect brick-wall characteristic would be used, something that can only be implemented in DSP. Also the experimental results show that different signal impairments like skew and quadrature error affect the EVM in different ways. It would be interesting to study how the measured EVM in these two cases correspong to BER in a real system.

The other approach which was discussed is using TR-EVM measurements and masks together with optical filtering. This is a good idea, since it would be possible both to say that a signal is faulty, and to identify exactly what is wrong with the signal. The testing could be done by counting mask hits. If there are too many mask hits, the TR-EVM plot could be studied closer to determine the source of the error. If there are no mask hits, the transmitter is ok. It is a simple procedure which could be done quickly in an industrial setting. The optical filtering could be done with a Waveshaper programmed with a Gaussian filter. The filter bandwidth would probably be chosen at a given fraction of the symbol rate, often 0.75×(symbol rate) or 0.5×(symbol rate) is used.

7.3 Future developments

The longer term goal is a new standard for testing 100 Gb/s PM-QPSK transmitters. If choosing the route with optical filtering, optical sampling, TR-EVM and masks for testing, the next step would be to develop masks which correlate well to required BER. This would have to be done experimentally in realistic fiber optic communication links. The design of the masks is outside the scope of this thesis.

The use of AWG:s for optical filtering of the signal was only discussed briefly. There are many advantages to filtering with AWG:s but as there was no AWG available for the experiments, this option was not investigated further. It could very well turn out to be a good solution to filter the signal in an AWG since it is built to filter out the frequencies of the WDM grid. The main advantages are that AWG:s are relatively cheap, well defined in standards, have a constant phase response and can be emulated in DSP.

Another interesting continuation of this study is to look at another way of optically filtering the signal. As was mentioned earlier in the report, it is possible to filter the pulses instead of the signal when using optical sampling. The end result should be the same and the insertion loss on the signal from the optical filter could be avoided. Using this method it would probably be easier to center the optical filter on the LO frequency accurately in an automated fashion. This method could also be used in order to design the receiver characteristics in a receiver based on optical sampling. This technique has not been investigated but would be interesting to look into.

References

[1] K. Kao and G. Hockham, "Dielectric-fibre surface waveguides for optical frequencies," *Electrical Engineers, Proceedings of the Institution of*, vol. 113, pp. 1151 –1158, july 1966.

[2] X. Zhou, J. Yu, M.-F. Huang, Y. Shao, T. Wang, P. Magill, M. Cvijetic, L. Nelson, M. Birk, G. Zhang, S. Y. Ten, H. B. Matthew, and S. K. Mishra, "32Tb/s (320x114Gb/s) PDM-RZ-8QAM transmission over 580km of SMF-28 Ultra-Low-Loss Fiber," in *Optical Fiber Communication Conference*, p. PDPB4, Optical Society of America, 2009.

[3] R. N. Hall, G. E. Fenner, J. D. Kingsley, T. J. Soltys, and R. O. Carlson, "Coherent Light Emission From GaAs Junctions," *Phys. Rev. Lett.*, vol. 9, pp. 366–368, Nov 1962.

[4] R. Mears, L. Reekie, I. Jauncey, and D. Payne, "Low-noise erbium-doped fibre amplifier operating at 1.54 um," *Electronics Letters*, vol. 23, pp. 1026 –1028, 10 1987.

[5] M. Sjödin, *Fiber-Optic Systems with Coherent Detection and Four-Dimensional Modulation.* Dissertation, Chalmers University of Technology, 2012.

[6] S. Savory, "Digital Coherent Optical Receivers: Algorithms and Subsystems," *Selected Topics in Quantum Electronics, IEEE Journal of*, vol. 16, pp. 1164 –1179, sept.-oct. 2010.

[7] British Standards Institution, "BS EN 61280-2-2:2008," 2008.

[8] E. Ip, A. P. T. Lau, D. J. F. Barros, and J. M. Kahn, "Coherent detection in optical fiber systems," *Opt. Express*, vol. 16, pp. 753–791, Jan 2008.

[9] C. Tang, H. Chen, F. Yin, M. Chen, and S. Xie, "200Gs/s real-time optical-sampling-based orthogonal frequency division multiplexing system," in *Optical Fiber Communication (OFC), collocated National Fiber Optic Engineers Conference, 2010 Conference on (OFC/NFOEC)*, pp. 1 –3, march 2010.

[10] R. Shafik, S. Rahman, and A. R. Islam, "On the Extended Relationships Among EVM, BER and SNR as Performance Metrics," in *Electrical and Computer Engineering, 2006. ICECE '06. International Conference on*, pp. 408 –411, dec. 2006.

[11] H. Sunnerud, M. Westlund, M. Sköld, and P. Andrekson, "Time-resolved error vector magnitude for transmitter mask testing in coherent optical transmission systems," in *Optical Fiber Communication Conference and Exposition (OFC/NFOEC), 2011 and the National Fiber Optic Engineers Conference*, pp. 1 –3, march 2011.

[12] I. Fatadin, S. Savory, and D. Ives, "Compensation of Quadrature Imbalance in an Optical QPSK Coherent Receiver," *Photonics Technology Letters, IEEE*, vol. 20, pp. 1733 –1735, oct. 2008.

[13] M. Taylor, "Phase Estimation Methods for Optical Coherent Detection Using Digital Signal Processing," *Lightwave Technology, Journal of*, vol. 27, pp. 901 –914, april, 2009.

[14] A. Viterbi, "Nonlinear estimation of PSK-modulated carrier phase with application to burst digital transmission," *Information Theory, IEEE Transactions on*, vol. 29, pp. 543 – 551, jul 1983.

[15] J. Johnson, D. Johnson, P. Boudra, and V. Stokes, "Filters using Bessel-type polynomials," *Circuits and Systems, IEEE Transactions on*, vol. 23, pp. 96 – 99, feb 1976.

[16] B. Saleh and M. Teich, *Fundamentals of photonics.* Wiley series in pure and applied optics, Wiley-Interscience, 2007.

[17] *Waveshaper 1000E User Manual, release C.*

[18] C. Pulikkaseril, L. A. Stewart, M. A. F. Roelens, G. W. Baxter, S. Poole, and S. Frisken, "Spectral modeling of channel band shapes in wavelength selective switches," *Opt. Express*, vol. 19, pp. 8458–8470, Apr 2011.

[19] M. Roelens, D. Williams, J. Bolger, and B. Eggleton, "Advanced applications of flexible ROADM technology," in *PhotonicsGlobal@Singapore, 2008. IPGC 2008. IEEE*, pp. 1 –4, dec. 2008.

[20] J. A. Dobrowolski, "Numerical Methods for Optical Thin Films," *Opt. Photon. News*, vol. 8, p. 24, Jun 1997.

[21] R. Pantoja, R. Souza, R. Rodrigues, G. Borges, C. Sales, and J. Costa, "Design of thin film filters using differential evolution optimization technique," in *Microwave and Optoelectronics Conference (IMOC), 2009 SBMO/IEEE MTT-S International*, pp. 447 –452, nov. 2009.

[22] ITU-T, "G.694.1, Spectral grids for WDM applications: DWDM frequency grid," 2012.

[23] J. Lazaro and J. Koppenborg, "New Phase Characterisation Method of AWG from Transmission and Group Delay Measurements," in *Optical Communication, 2002. ECOC 2002. 28th European Conference on*, vol. 3, pp. 1 –2, sept. 2002.